Local atomic and electronic structure in the LiVPO4(F,O) tavorite-type materials from solid-state NMR combined with DFT calculations

Tahya Bamine, Edouard Boivin, Christian Masquelier, Laurence Croguennec, Elodie Salager, Dany Carlier

Local atomic and electronic structure in the $LiVPO_4(F,O)$ Tavorite-type materials from Solid State NMR combined with DFT calculations

Tahya Bamine[a,b], Edouard Boivin[a,b,d], Christian Masquelier[b,c,d], Laurence Croguennec[a,b,c], Elodie Salager[b,e], and Dany Carlier[a,b,c*]

[a] *CNRS, Univ. Bordeaux, Bordeaux INP, ICMCB UMR 5026, F-33600 Pessac, France*
[b] *RS2E, Réseau Français sur le Stockage Electrochimique de l'Energie, FR CNRS 3459, F-80039 Amiens Cedex 1, France*
[c] *ALISTORE-ERI, FR3104, 80039 Amiens cedex, France*
[d] *Laboratoire de Réactivité et de Chimie des Solides, UMR CNRS 7314, Université de Picardie Jules Verne, F-80039 Amiens Cedex 1, France*
[e] *CNRS, CEMHTI UPR 3079, Université d'Orléans, Orléans, France*

Abstract

^{7}Li, ^{31}P and ^{19}F solid state NMR spectroscopy was used to investigate the local arrangement of Oxygen and Fluorine in $LiVPO_4F_{1-y}O_y$ materials, interesting as positive electrode materials for Li-ion batteries. From the evolution of the 1D spectra versus y, 2D ^{7}Li RFDR experiments combined and a tentative signal assignment based on DFT calculations, it appears that F and O are not randomly dispersed on the bridging X position between two X-VO_4-X octahedra (X = O or F), but tend to segregate at a local scale. Using DFT calculations, we analyzed the impact of the different local environments on the local electronic structure. Depending on the nature of the VO_4X_2 environments, vanadium ions are either in the +III or in the +IV oxidation state and can exhibit different distributions of their unpaired electron(s) on the d orbitals. Based on those different local electronic structures and on the computed Fermi contact shifts, we discuss the impact on the spin transfer mechanism on adjacent nuclei and propose tentative signal assignments. The O/F clustering tendency is discussed in relation with the formation of short V^{IV}=O vanadyl bonds with a very specific electronic structure and possible cooperative effect along the chain.

Keywords

NMR, ^{7}Li, ^{31}P, ^{19}F, DFT, solid-state, paramagnetic, RFDR, Fermi contact shift, Li-ion battery, electrode material.

Introduction

Among the wide varieties of $LiMXO_4Y$ tavorite-type compositions with M = V, Fe, Mn or Ti, and X = P or S [1], vanadium-based $LiVPO_4F$ and $LiVPO_4O$ (Figure 1) appear to be the most attractive ones as positive-electrode materials for lithium-ion batteries. Indeed, they exhibit high working voltages (i.e., 4.26 and 3.95 V vs Li^+/Li, respectively) and thus high theoretical energy densities with the exchange of one electron per vanadium [2]. Nevertheless, among the numerous studies reporting on apparently pure $LiVPO_4F$, discrepancies in the average crystal structure and electrochemical properties are observed [2-5]. Using 2D ^7Li MAS NMR we evidenced the presence of defects in $LiVPO_4F$ [6] whose amounts may vary according to the synthesis conditions. Following this work, we identified the nature of the defects using ^7Li MAS NMR combined with DFT calculations [7]: F^- ions are substituted locally by O^{2-}, thus forming V^{4+} ions involved in a vanadyl bond with a very specific electronic structure that modifies the Fermi contact shifts observed for adjacent Li^+ ions. Recently, Kang and co-workers reported a $LiVPO_4F_{\sim 0.25}O_{\sim 0.75}$ phase, whose average structure is similar to that of $LiVPO_4F$ (despite the large O^{2-}/F^- substitution ratio) showing the possibility of extended substitution of fluorine by oxygen [5]. In a recent study, we synthesized several $LiVPO_4F_{1-y}O_y$ phases with control of the substitution ratio of oxygen for fluorine in order to study the influence of vanadyl-type defects on the average structure as well as on the local environment around vanadium [8]. The concentration of vanadyl-type defects was shown to have a strong influence on the electrochemical behavior in terms of redox processes involved, energy density, cyclability and rate capability [8, 9]. A better understanding of the local structural arrangement is of prime importance for further material optimization.

The $LiVPO_4F$ and $LiVPO_4O$ structures are not described in the same model, due to the presence of vanadyl bonds (i.e. short V^{IV}=O bonds) along the chains in $LiVPO_4O$ that requires a unit cell twice larger than the one used for $LiVPO_4F$ (Figure 1). As described in Ref. [8] all the intermediate compositions $LiVPO_4F_{1-y}O_y$ ($y < 0.9$) can be described considering a $LiVPO_4F$-type model. No superstructure peaks were observed suggesting thus a disordered sequence of V^{III} and V^{IV} (involved in vanadyl V^{IV}=O bond) along the chains. Nevertheless, the presence of microstrains and the deviation from the Vegard's law for the cell parameters have suggested a possible clustering along the chains, without long-range ordering.

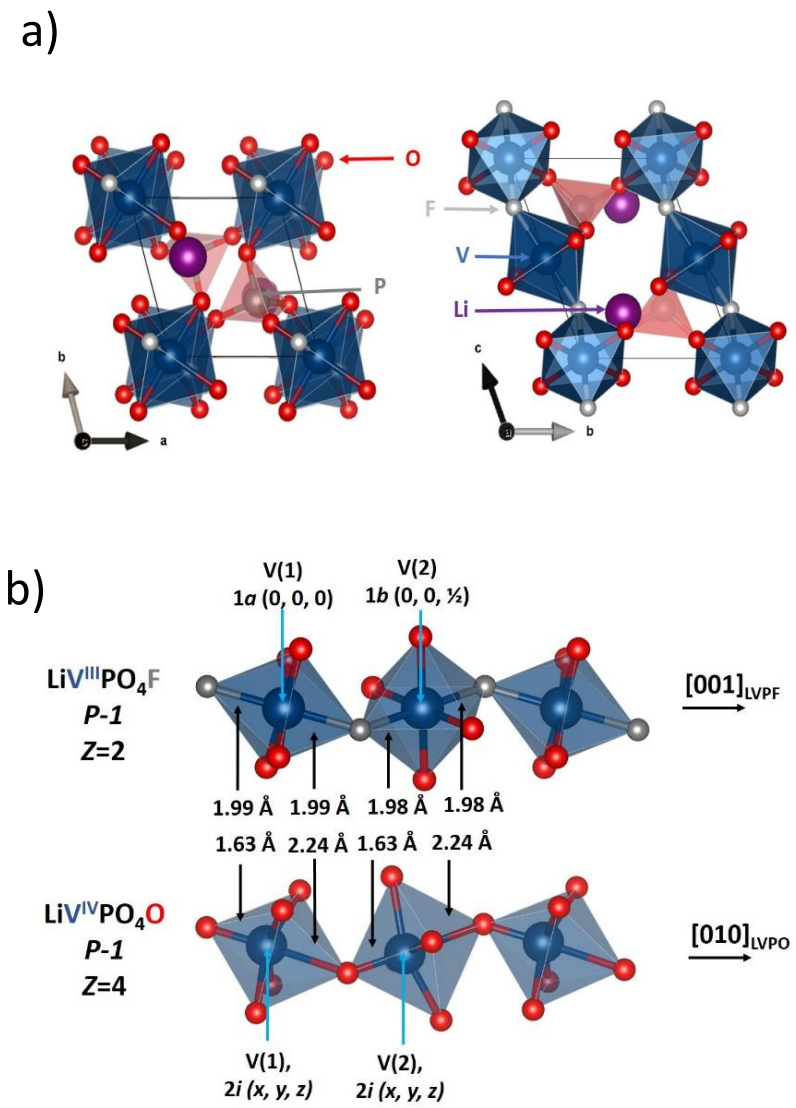

***Figure 1**: a) Structure of $LiVPO_4F$ along the [001] (left) and the [100] (right) directions: VO_4F_2 octahedra in blue, PO_4 tetrahedra in red and lithium in purple. b) V-F and V-O distances along the chains of vanadium octahedra in $LiVPO_4F$ and in $LiVPO_4O$.*

As diffraction gives access only to an average long-range description, no in-depth information on the V− F bonds facing the vanadyl-type bonds (in F− (V^{IV}=O)) and on the V− O bonds facing the V− F ones (in O− (V^{III}− F)) can be obtained from this technique. From IR and XAS studies, we evidenced that vanadyl bonds were locally formed in agreement with the predictions of DFT calculations [7]. However, those characterization techniques did not allow to investigate the possibility of clustering which might be expected if one considers cooperative effect due to the alternation of short and long bonds along the chains. Using Magic Angle

Spinning (MAS) NMR techniques combined with DFT calculations we investigate, in this paper, the local atomic and electronic structure in those materials.

Experimental part

The mixed valence (i.e. V^{III}/V^{IV}) $LiVPO_4F_{1-y}O_y$ phases were obtained through one-step solid-state syntheses as described in Ref. [8] from V_2O_5, LiF and H_3PO_4 precursors. Three mixed valence compositions were prepared: $LiVPO_4F_{0.65}O_{0.35}$, $LiVPO_4F_{0.45}O_{0.55}$ and $LiVPO_4F_{0.25}O_{0.75}$. In order to confirm the fluorine content obtained which is, assuming the $LiVPO_4F_{1-y}O_y$ composition, related to the average oxidation state of vanadium, the magnetization of all materials were measured as a function of temperature in the paramagnetic domain. Quasi-stoichiometric $LiVPO_4F$ was synthesized through a two-step carbothermal reduction as described previously [2] from V_2O_5 reduced by a small excess of C_{SP} carbon in the presence of $NH_4H_2PO_4$ and addition of LiF. $LiVPO_4O$ was synthesized by a solid-state reaction as described in Ref. [8] from V_2O_3, Li_3PO_4 and $NH_4H_2PO_4$ precursors.

^{7}Li MAS NMR spectra were recorded on a Bruker Avance III spectrometer with a 7 T magnet (116 MHz resonance frequency for ^{7}Li). A standard Bruker 2.5 mm MAS probe at a 30 kHz spinning frequency was used. A Hahn echo sequence synchronized with one rotor period was used with a 90° pulse of 1.2 µs and a recycling delay of 2s. 1M LiCl aqueous solution was used as 0 ppm external reference. ^{31}P *ss*-NMR spectra were acquired on a Bruker Avance III spectrometer with a 2.35 T magnetic field at a resonance frequency of 40.6 MHz by using a standard Bruker 2.5 mm magic-angle spinning (MAS) probe with a 30 kHz spinning frequency. A Hahn echo sequence synchronized with one rotor period was applied with a 90^o pulse of 1.1 μs and a recycle delay of 1 s. H_3PO_4 85% (Sigma-Aldrich) was used as external reference for 0 ppm chemical shift. ^{19}F *ss*-NMR spectra were acquired on a Bruker Avance III spectrometer with a 2.35T magnetic field at a resonance frequency of 94.3 MHz by using a standard Bruker 2.5 mm magic-angle spinning (MAS) probe with a 30 kHz spinning frequency. A Hann echo sequence synchronized with one rotor period was applied with a 90^o pulse 1.0 μs and a recycle delay of 1 s. A $CFCl_3$ (1M) solution was used as external reference for 0 ppm chemical shift.

Extra ^{7}Li NMR experiments were performed at the French national platform IR-RMN-THC FR3050 CNRS (Orléans, France), on a Bruker Avance III spectrometer with a 17.6 T magnet (291.5 MHz resonance frequency for ^{7}Li) and a wide-bore Bruker 1.3 mm MAS probe with a spinning rate of 64 kHz. The chemical shifts were referenced to an aqueous 1 mol.L^{-1} LiCl solution. Two-dimensional ^{7}Li-^{7}Li EXSY and fp-RFDR correlation spectra were recorded with a repetition time of 50 ms (sufficient for relaxation of the signals of interest- peaks 2 and 4 are saturated) and a RF power of 98.3 W (208 kHz). The other conditions were similar to those used for the study published earlier [6]. All spectra were processed with an exponential filter (line broadening 200 Hz) using the Topspin software. The spectra were then imported in Matlab (The MathWorks Inc) using a home-made script for plotting the figures with controlled contours and color-code.

Fermi contact shift that are mainly responsible for the shifts observed for paramagnetic materials can be expressed as:

$$\delta_{iso}^{i}(T) = \frac{1}{3SN_A}\rho^{i}(0)\chi_M(T) \qquad \text{eq. (1)}$$

where S is the spin quantum number of the paramagnetic ion, $\rho^{i}(0)$ is the electronic spin density on the *i* nucleus and χ_M the experimental molar magnetic susceptibility (at the temperature of the NMR measurement, here 320 K while spinning at 30 kHz). First principles calculations were used to compute the electronic spin density at the probe nucleus within the Density Functional Theory (DFT) framework. The standard PAW-PBE potentials as implemented in the Vienna ab initio Simulation Package (VASP) code [10] were used for O, P, and V whereas the "sv" PAW-PBE potential that treats the 1s shell as valence states was chosen for Li [10]. All calculations were spin polarized type with a ferromagnetic type ordering which is considered appropriate for the Fermi contact shift, as described in reference [11]. A plane wave energy cut-off of 600 eV and a k-mesh dense enough to reach convergence were used. Generalized Gradient Approximation + U (U = 4.0 eV) approach, where Hubbard type interaction is added to localize 3d electrons, was used. In our previous study on $LiVPO_4F$, several values were used for the U term: as 4 eV led to good agreement between calculated and experimental shifts it has been chosen in the present study (ref [7]). Further details concerning the Fermi contact shifts calculations using this method can be found in ref [7, 12-13]. To model the substituted phases, several O/F arrangements based on a 128-atom supercell (2a x 2b x 2c) were used for $LiVPO_4F_{0.25}O_{0.75}$, $LiVPO_4F_{0.5}O_{0.5}$ or $LiVPO_4F_{0.75}O_{0.25}$ compositions. The structure of the supercell was relaxed using GGA+U, and the different local electronic

structures were analyzed. 3D calculated spin density maps were plotted using the VESTA software (Visualization for Electronic and Structural Analysis) [14].

Results and discussion

Figure 2a shows the ^{7}Li MAS NMR spectra recorded for five $LiVPO_4F_{1-y}O_y$ samples with y = 0, 0.35, 0.55, 0.75 and 1. A rather sharp signal (#4) centered at 115 ppm is observed for $LiVPO_4F$, in agreement with previous publications [15-16] and is attributed to the unique Lithium site identified by diffraction [2].

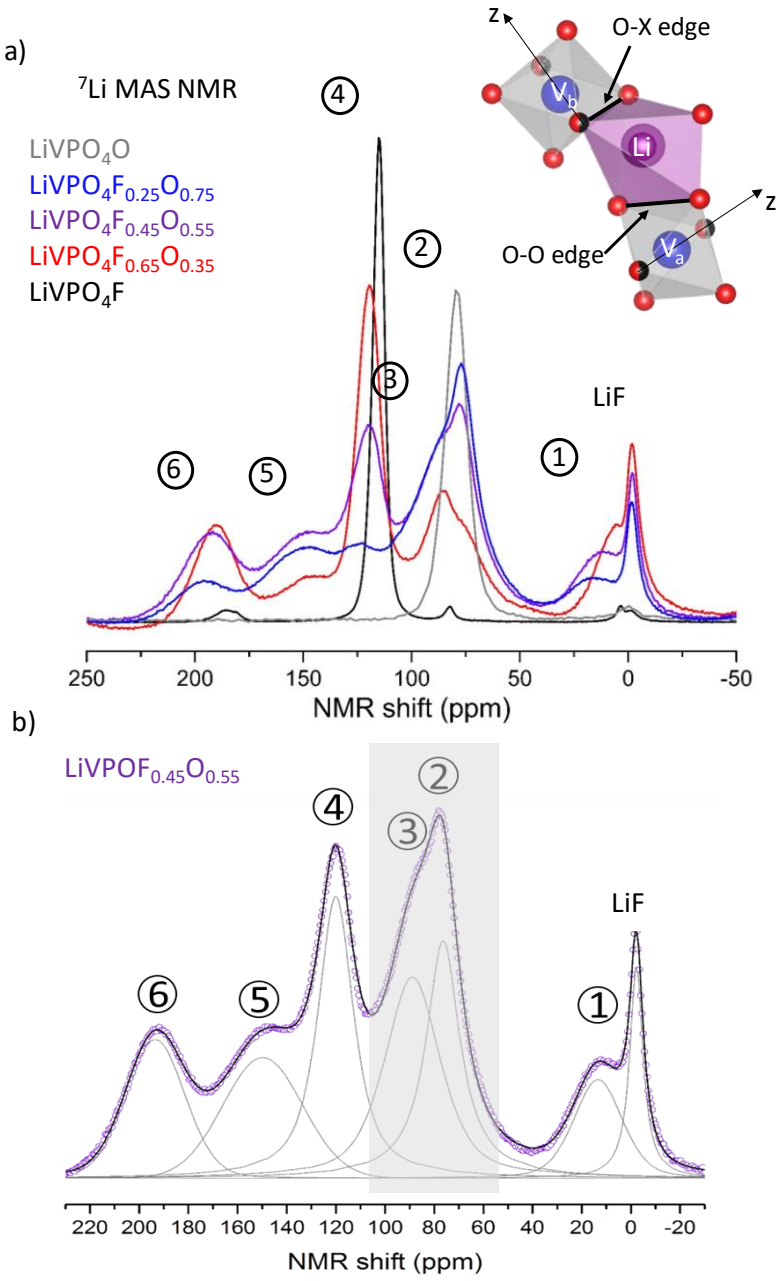

***Figure 2**: a) ^{7}Li MAS NMR spectra of the series of five LiVPO$_4$F$_{1-y}$O$_y$ compositions. The global intensity of the signals obtained for the two end members phases, LiVPO$_4$F and LiVPO$_4$O, has been divided by 10. In inset, a schematic illustration of the lithium environment vs. V_a and V_b octahedra (V octahedra sharing an edge with Li polyhedra are only depicted); V_a and V_b do not belong to the same chain; positions in red = O, positions in red/black = O or F (bridging position). The z-axis indicates the direction of the vanadyl bonds, when present. The different signals observed are labelled 1 to 6 to facilitate the discussion in the text. b) Tentative decomposition of the 1D ^{7}Li MAS NMR spectra of LiVPO$_4$F$_{0.45}$O$_{0.55}$ phase using 6 contributions with a pseudo voigt lineshape in addition to the LiF contribution around 0 ppm. Note that especially in the grey regions with strong overlap, more contributions could have been considered.*

The spectrum for the $LiVPO_4F$ sample also exhibits a weak signal at -1 ppm assigned to the presence of residual LiF and other additional signals at 4 ppm (peak #1), 84 ppm (peak #3) and 186 ppm (peak #6) which have been assigned, based on DFT calculations, to vanadyl-type defects [7]. The examination of the NMR spectrum of $LiVPO_4O$ shows a single sharp peak at 79 ppm (peak #2). In $LiVPO_4O$, as there are two crystallographic sites for Lithium [17], two ^{7}Li MAS NMR signals would have been expected. In our conditions, we, however observe only one signal, probably due to the high structural similarity between both sites and/or to fast lithium mobility between them. Note that a Fermi contact shift calculation indeed predicts two very similar shifts for the two Li sites (for more details see Figure S1 in supplementary information).

For all the Tavorite-type phases discussed here, the lithium-coordination polyhedra share two edges and two separate corners with four VO_4X_2 octahedra, with X being an O or F anion. The e_g orbitals of vanadium being empty (i.e. t_{2g}^2 for V^{III} and t_{2g}^1 for V^{IV}), the main spin transfer from vanadium to lithium leading to the Fermi contact shift occurs from the t_{2g} orbitals pointing towards common edges between the LiO_4X and VO_4X_2 polyhedra (i.e. an O-O edge and an O-X edge, X = bridging anion, O or F). This simplified lithium environment is depicted in the inset of **Figure 2a**. The two vanadium sites sharing an edge with the Li polyhedra are labeled V_a and V_b depending on the nature of the common edge (O-O for V_a and O-X (X = O or F) for V_b) and don't necessarily correspond to the V(1) and V(2) crystallographic sites. Note that V_a and V_b do not belong to the same chain.

For $LiV^{III}PO_4F$, the two d electrons are homogeneously distributed in the three t_{2g} orbitals. The spin transfer is strong due to the local electronic structure and to the contribution of both vanadium octahedra sharing an edge with the lithium polyhedra [7]. In the case of $LiV^{IV}PO_4O$, the presence of vanadyl bonds along the z direction, indicated in the inset of Figure 2, induces a lift of degeneracy of the t_{2g} orbitals: the d_{z2} and one of the d_{xz}/d_{yz} orbitals are involved in the strong covalent V^{IV}=O vanadyl bond, while the d_{xy} orbital is stabilized and is the one carrying the unpaired electron [7;12] (as described in Figure S2 in supplementary information). Therefore, in $LiVPO_4O$ a spin transfer mechanism from V^{IV} to Li can occur only from the d_{xy} orbital through the O-O edge shared with V_a (see **Figure 2a**). The orientation of the V_b site and

its electronic configuration do not allow the possibility of such spin transfer as discussed in Ref [7].

The mixed valence V^{III}/V^{IV} $LiVPO_4F_{1-y}O_y$ samples exhibit ^7Li NMR spectra with very broad contributions located in the neighboring of the signals observed for $LiVPO_4F$ (isotropic peak and defects contributions) and $LiVPO_4O$. Actually at least six components can be distinguished, in addition to a quasi-non-shifted peak at -1 ppm (denoted as LiF in **Figure 2**), as can be seen on the tentative decomposition of the spectra (**Figure 2b** and **Figure S3** for the other spectra). The presence of residual LiF was also confirmed ^{19}F NMR spectra, as discussed below. Note that the ^7Li spectrum obtained for the $LiVPO_4F_{0.25}O_{0.75}$ sample is really similar to the spectrum recently reported by Parapari et al. for a sample prepared from $LiVPO_4O$ and LiF heated at 800°C for 1h [18]. By analogy with the end-member phases, two contributions can be assigned: the signal around 120 ppm (#4) assigned to Li in interaction with two F-V^{III}-O_4-F octahedra ($LiVPO_4F$-like environment) and the signal around 75 ppm (#2) assigned to Li in interaction with two O-$V^{IV}O_4$-O octahedra ($LiV^{IV}PO_4O$-type contribution).

In order to assign the remaining signals observed around 10 ppm (#1), 85 ppm (#3), 150 ppm (#5) and 195 ppm (#6), DFT calculations were performed with structural models taking into account several F/O and V^{III}/V^{IV} spatial distributions for the $LiVPO_4F_{0.75}O_{0.25}$, $LiVPO_4F_{0.5}O_{0.5}$ and $LiVPO_4F_{0.25}O_{0.75}$ compositions. Indeed, using large supercells, we were able to distribute F and O differently on the X positions of VO_4X_2 octahedra so that very homogeneous cells as well as "clustered" ones were considered. From the corresponding Fermi contact shift calculations for the ^7Li atoms, a complete assignment of the signals is not trivial since several Li environments with V^{III}/V^{IV} either in V_a or V_b sites lead to rather similar shifts. To that end, in Figure S4, we summarize the different oxidation states and electronic structures that were found theoretically depending on the V local environments vs. O/F. We also indicate the expected spin transfer (ST) on an adjacent Li, stronger or weaker compared to the one expected from V^{III} in $LiVPO_4F$. As intuitively expected, we do not observe the formation of a V^{3+} ion in a O-VO_4-O (VO_6) octahedron nor the formation of a V^{4+} ion in a F-VO_4-F one (VO_4F_2). For the VO_6 environment, whatever the nature of the adjacent VO_4X_2 octahedra, the formation of a short V=O bond is observed after structural optimization along the local z direction and the V^{4+} ions exhibit the same electronic structure as in $LiVPO_4O$: d_{xy}^1. If V^{IV} is in a V_b position, no spin transfer toward the adjacent Li is expected whereas if it is in V_a a strong spin transfer is expected (**Figure 3**). For the VO_4F_2 environment, depending on the nature

of the adjacent VO_4X_2 octahedra, the electronic structure of the V^{III} differs: either the three t_{2g} orbitals are partially occupied as in $LiVPO_4F$, or only the d_{xz} and d_{yz} orbitals are carrying the spins. In both cases, a spin transfer similar to the one observed in $LiVPO_4F$ is expected toward the Li site sharing an edge [7]. For the O-VO_4-F environment, the vanadium ions can be +III or +IV depending on the nature of the adjacent VO_4X_2 octahedra, with various predicted spin transfer magnitudes depending on the nature of the V sites, V_a and V_b, and on their electronic spin structures (Figure S4).

As Li polyhedra is sharing an edge with one $V_aO_4X_2$ polyhedron and another with one $V_bO_4X_2$ site as represented in **Figure 2a**, two types of spin transfer may occur. Based on the Fermi contact shifts calculations we propose in **Table I** the tentative assignments of the ^{7}Li signals for the various $LiVPO_4F_{1-y}O_y$ phases.

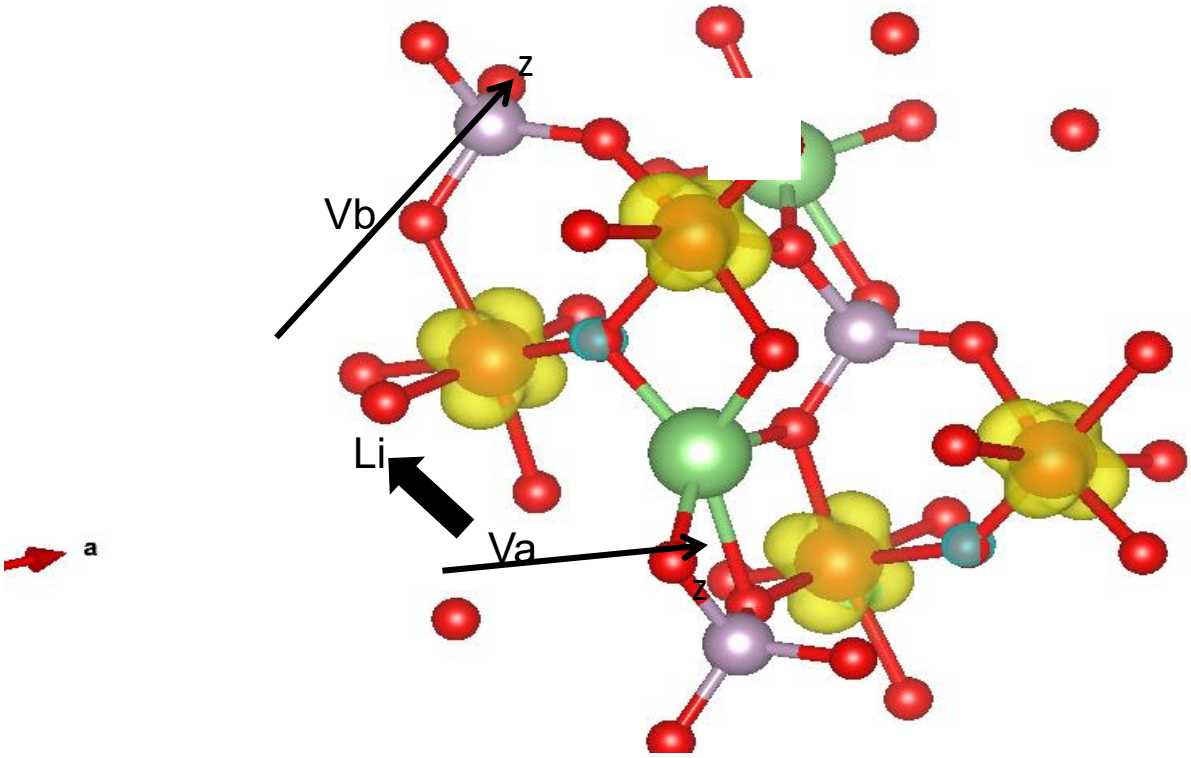

***Figure 3**: Calculated 3D spin density map around Li in $LiVPO_4O$ showing the local electronic structure of the two V^{4+} ions in VO_6 octahedra sharing an edge with the LiO_5 polyhedra. A V^{4+} ion located in a V_a site can transfer spin density on Li as the d_{xy} orbital carrying the unpaired electron is properly oriented, but no spin transfer is expected from a V^{4+} ion in a V_b site.*

Signal label	Proposed corresponding Li Environment		Calculated Fermi contact shifts range (ppm)	
	Va	Vb		
1	F-V^{IV}-O	O-V^{IV}-O	[10-30]	
2	O-V^{IV}-O	O-V^{IV}-O	[60-100]	Similar to $LiVPO_4O$
3	O-V^{IV}-O or F-V^{IV}-O	F-V^{IV}-O	[50-130]	
4	F-V^{III}-F	F-V^{III}-F	[120-140]	Similar to $LiVPO_4F$
5	F-V^{III}-F or F-V^{III}-O	F-V^{III}-F or F-V^{III}-O	[100-200]	
6	O-V^{IV}-O	F-V^{III}-F	[150-250]	

***Table I**: Tentative assignment of the ^{7}Li MAS NMR signals to the different Li environments versus V^{III} and V^{IV} in Va and Vb sites, based on Fermi contact shifts calculated for the models taking into account the different distribution of O and F in the X (bridging) position. For more clarity the different VO_4X_2 octahedra are denoted by X-V^{III}-X or X-V^{IV}-X with X = O or F.*

As the ^{7}Li signals from environments near V^{4+} or V^{3+} are overlapping, it was not possible to discuss further the local arrangement in the $LiVPO_4F_{1-y}O_y$ series, based on the evolution of the signals intensity versus y, that would have T2 measurements for the different Li sites in our Hahn echo conditions. We therefore used 2D ^{7}Li NMR experiments to investigate the possibility of a partial clustering of V^{4+}-rich and V^{3+}-rich domains in similar conditions to those reported by Messinger *et al*. in ref [6] for the detection of vanadyl type defects in $LiVPO_4F$. Finite pulse radiofrequency driven recoupling (fp-RFDR) [19,20] is implemented during the mixing time of a two-dimensional ^{7}Li-^{7}Li experiment to reintroduce the homonuclear dipolar couplings otherwise averaged out by MAS. Such dipolar couplings can usually be reintroduced for distances less than 1 nm, and are therefore a marker of spatial proximity at the nanometer scale.

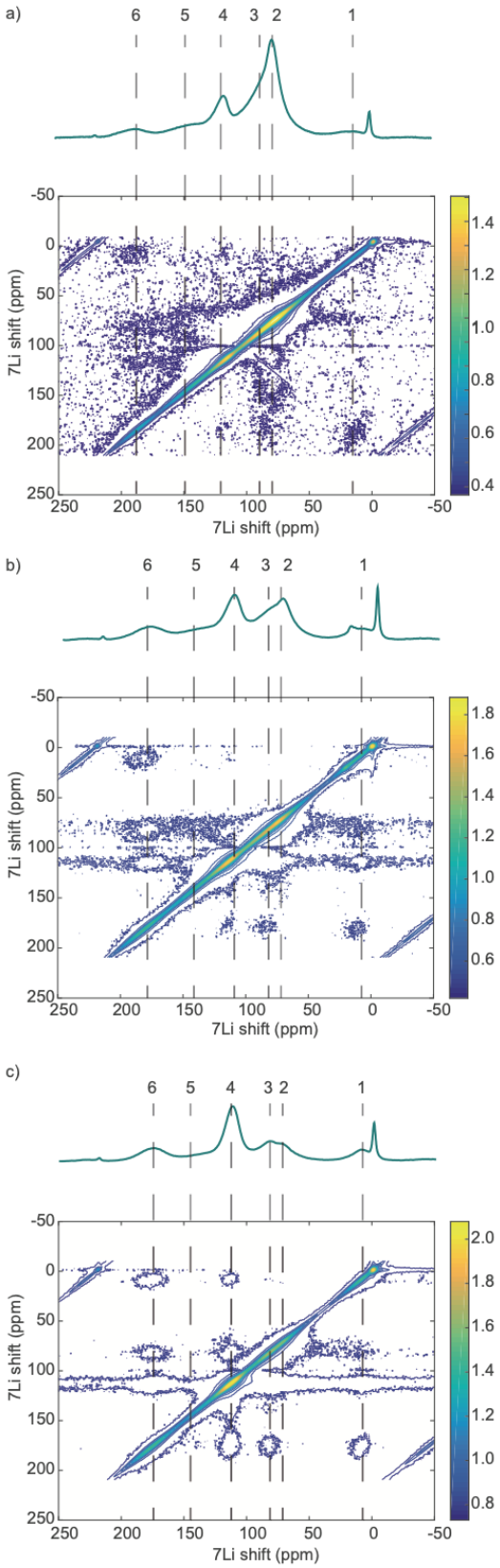

Figure 4: *^{7}Li-^{7}Li fp-RFDR correlation spectra with a mixing time of 5 ms for a) $LiVPO_4F_{0.25}O_{0.75}$, b) $LiVPO_4F_{0.45}O_{0.55}$ and c) $LiVPO_4F_{0.65}O_{0.35}$. The ^{7}Li spectrum of the corresponding phase after the RFDR mixing (no t_1 evolution) is displayed on top of each 2D correlation plot.*

Figure 4 shows the ^{7}Li-^{7}Li fp-RFDR correlation spectra for the three intermediate compositions, namely $LiVPO_4F_{0.25}O_{0.75}$, $LiVPO_4F_{0.45}O_{0.55}$ and $LiVPO_4F_{0.65}O_{0.35}$. Cross-peaks are observed between the components previously labelled 1, 3, 4 and 6 for all compositions, although much fainter in $LiVPO_4F_{0.25}O_{0.75}$. These cross-peaks are absent in EXSY experiments run in the same conditions (see **Figures S5, S6, S7**) and are therefore assigned to proximity in space rather than to chemical exchange or mobility of the Li ions. The Li environments leading to signals #1, #3 and #6, arise from the defects in close proximity with the Li environment $LiVPO_4F$-type (signal #4) as demonstrated in our previous work [6]. Interestingly, this clustering of the defects with the $LiVPO_4F$-type environment is still observed (although less easily) in the F-poor composition. We tested a range of mixing times (from 1 ms to 10 ms, see Figures S6, S7, S8) to probe shorter and longer distances and did not detect any cross-peaks for Li environments leading to signal #5 and to signal #2 ($LiVPO_4O$-type). We therefore conclude that they are isolated for the three compositions probed in this work.

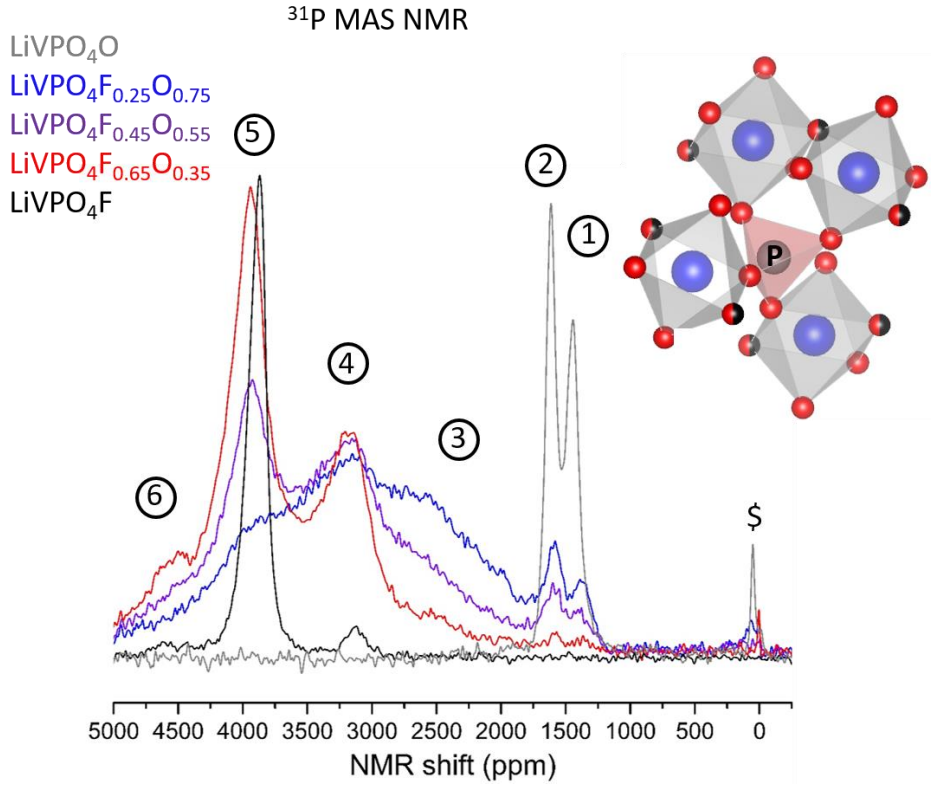

***Figure 5**: ^{31}P MAS NMR spectra of the series of five $LiVPO_4F_{1-y}O_y$ compositions. The global intensity of the signal obtained for the end members phases, $LiVPO_4F$ and $LiVPO_4O$, have been divided by 10. In inset, a schematic illustration of the Phosphorous environment vs. V octahedra; positions in red = O, positions in red/black = O or F (bridging position). The different signals observed are labelled 1 to 6 to facilitate the discussion in the text. $ = signal assigned to a diamagnetic impurity.*

Figure 5 shows the ^{31}P MAS NMR spectra recorded for the series of $LiVPO_4F_{1-y}O_y$ compositions. In Tavorite-type structures, the PO_4 tetrahedra are connected to four different transition metal octahedra via the oxygen belonging to the VO_4 plane of these octahedra. As also discussed by Castets et al. for the $LiMPO_4OH$ tavorite series, in our case (i.e. $t_{2g}^2e_g^0$ or $t_{2g}^1e_g^0$) the spin transfer to the 2s (or the sp^3 hybrid) orbital of Phosphorus occurs from the t_{2g} orbitals (via π overlap with a p orbital of oxygen) [21]. In $LiVPO_4F$, two ^{31}P MAS NMR signals are observed: one located at 3871 ppm (#5 in **Figure 5**) and a second one, weaker and unresolved due to the overlap with a spinning side band, located at larger shifts (#6). That latter isn't expected regarding the unique phosphorous site in the structure and could correspond to the defects' contribution (better seen by ^7Li NMR). The two signals at 1613 ppm and 1441 ppm (#1 and #2) observed for $LiVPO_4O$ confirm the existence of two crystallographic sites in this phase. Based on the DFT Fermi contact shift calculations we can assign the most shifted signal to P(1) and the less shifted one to P(2) (Figure S1) (P(1) and P(2) designation being similar to ref [2]). The ^{31}P NMR spectra of the other $LiVPO_4(O,F)$ phases with V^{3+} and V^{4+} are overall very broad due to the large amount of possible P environments versus V^{3+}/V^{4+} with different electronic structures as summarized in Figure S4. Nevertheless, we can assign signals #1/#2 and #5 to P environments close to those observed in $LiVPO_4O$ and $LiVPO_4F$ respectively. The signals #3, #4 and #6 can be assigned then to P surrounded by both V^{3+} and V^{4+} ions in different VO_4X_2 sites, therefore with various electronic structures as depicted in Figure S4. A further analysis of the ^{31}P spectra is delicate considering the overall broadening of the signals that strongly overlap.

Contrarily to ^7Li and ^{31}P NMR, ^{19}F nuclei are surrounded by two vanadium ions of the same chain (**Figure 1**), that are obviously in F-VO_4-X octahedra. Therefore, ^{19}F NMR may be the most relevant probe to investigate the possibility of V^{3+} or V^{4+} clusters formation within a chain that would result from a cooperative effect of the vanadyl bond formation with alternation of long and short V-O distances along the chain. Consequently, the four ^{19}F MAS NMR spectra of the $LiVPO_4F_{1-y}O_y$ series are compared in **Figure 6**.

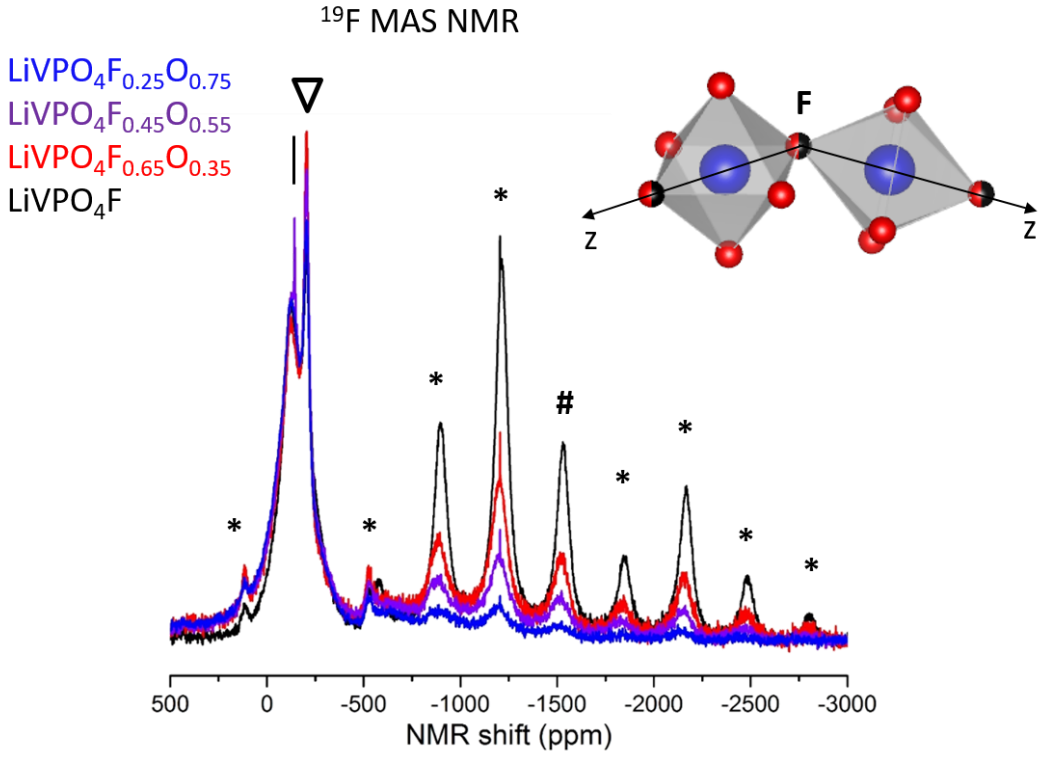

***Figure 6**: [19]F MAS NMR spectra of the series of four $LiVPO_4F_{1-y}O_y$ compositions with the isotropic peak highlighted by # and the spinning side bands by *. The additional signals assigned to LiF and to the probe contribution are marked as ∇ and | respectively. In inset, a schematic illustration of the Fluorine environment vs. V octahedra; positions in red = O, positions in red/black = O or F (bridging position).*

These spectra exhibit a strong parasitic contribution from the probe (which contains Teflon) around -150 ppm and from an LiF impurity at -208 ppm. The isotropic peak is located at -1500 ppm for $LiVPO_4F$ and all other contributions regularly separated are assigned to spinning side bands [7]. Surprisingly, no other peak which could be assigned to a Fluorine nucleus in interaction with V^{4+} cations can be detected for mixed valence samples. We expected a weak spin transfer from V^{4+} to F since the electronic spin located in the d_{xy} orbital is not pointing toward F. For the $LiVPO_4F_{1-y}O_y$ series only a slight shift (around 10 ppm) and a slight broadening of the ^{19}F signal is detected. The global intensity of this signal decreases gradually with the substitution of F by O. Nevertheless, due to the presence of the probe signal that may overlap with spinning side bands, the precise integration of the NMR signal cannot be performed. This study, however, shows that a negligible number of $F\text{-}V^{IV}\text{-}O$ environments exist along the chain that corroborates the clustering tendency of O in the vanadium chain, with the formation of O-rich (therefore V^{4+}-rich) domains and F-rich (therefore V^{3+}) ones.

Conclusion

Multinuclear solid-state NMR was used to investigate the local arrangement of oxygen and fluorine in the bridging X position of the vanadium VO_4X_2 octahedra along the chains in the $LiVPO_4F_{1-y}O_y$ series. The evolution of the ^{7}Li, ^{31}P and ^{19}F 1D spectra and the 2D ^{7}Li fp-RFDR experiments performed along the series indicates that F and O are not randomly dispersed on the X position in the $LiVPO_4F_{1-y}O_y$ materials, but tend to segregate at a local scale. This can be induced by the formation of short V^{IV}=O bonds that would be more stable if a cooperative effect was possible with alternating long V^{IV}-O and short V^{IV}=O bonds. This would result in O-$V^{IV}O_4$-O-rich domains and F-$V^{III}O_4$-F-rich ones along the chains. Using DFT calculations on model compounds, we analyzed the impact of the different local environments on the local electronic structure. Depending on the nature of the VO_4X_2 environments, vanadium ions are in the +III or +IV oxidation states and can exhibit different repartitions of their unpaired electron(s) on the d orbitals. Based on that range of local electronic structures and computed Fermi contact shifts, we could then discuss the impact of the spin transfer mechanism on adjacent nuclei and propose tentative signal assignments.

The O/F clustering tendency observed here is in good agreement with the observation of microstrains and deviations from the Vegard's law for the solid solution $LiVPO_4F_{1-y}O_y$ reported in our previous study. The present study is a first step to better understand the complex redox behavior observed for the $LiVPO_4F_{1-y}O_y$ materials in Li cells with the activation of the V^{IV}═O/V^{V}═O redox couple during the first step of the charge, and then upon further Li^+ extraction the activation of the V^{3+}/V^{4+} redox couple in fluorine-rich environments [9], that may result from the complex electronic structure and clustering tendency observed.

Acknowledgments

The authors acknowledge FEDER, the Région Hauts-de-France and the RS2E Network for the funding of EB's PhD thesis, as well as the financial support of Région Nouvelle Aquitaine and of the French National Research Agency (STORE-EX Labex Project ANR-10-LABX-76-01 and HIPOLITE Progelec project ANR-12-PRGE-0005-02). Financial support from the IR-RMN-THC Fr3050 CNRS for conducting the research is also gratefully acknowledged, as well as the Mésocentre de Calcul Intensif Aquitain (MCIA) and the modelling centre (ISM) for computing facilities. P. Aurel (ISM) is acknowledged for technical assistance.

References:

[1] C. Masquelier, L. Croguennec, *Chem. Rev*. **2013**, *113 (8)*, 6552−6591.

[2] J-M. Ateba-Mba, C. Masquelier, E. Suard, L. Croguennec, *Chem. Mater.* **2012**, *24*, 1223−1234.

[3] J. Zheng, B. Zhang, Z. Yang, *J. Power Sources* **2012**, *202*, 380−383.

[4] P-F. Xiao, M-O. Lai, L. Lu, *Solid State Ionics* **2013**, *242*, 10−19.

[5] M. Kim, S. Lee, B. Kang, *Chem. Mater.* **2017**, *29 (11)*, 4690−4699.

[6] R. Messinger, R. M. Ménétrier, E. Salager, A. Boulineau, M. Duttine, D. Carlier, J-M Ateba Mba, L. Croguennec, C. Masquelier, D. Massiot; M. Deschamps, *Chem. Mater.* **2015**, *27*, 5212−5221.

[7] T. Bamine, T. E. Boivin, F. Boucher, R. Messinger, E. Salager, M. Deschamps, C. Masquelier, L. Croguennec, M. Ménétrier, D. Carlier, *J. Phys. Chem. C* **2017**, *121 (6)*, 3219−3227.

[8] E. Boivin, R. David J-N. Chotard, T. Bamine, A. Iadecola, L. Bourgeois, E. Suard, F. Fauth D. Carlier, C. Masquelier, L. Croguennec, *Chem. Mater.* **2018**, *30*, 5682−5693

[9] E. Boivin, A. Iadecola, F. Fauth, D. Carlier, J-N. Chotard, C. Masquelier, L. Croguennec *Chem. Mater.* **2019**, *31 (18)*, 7367-7376.

[10] G. Kresse, J. Furthmüller, *Computational Materials Science* **1996**, *6*, 15–50.

[11] D. Carlier, M. Ménétrier, C.P. Grey, C. Delmas, G. Ceder, *Phys. Rev. B* **2003**, *67*, 174103.

[12] L-H-B Nguyen, P. Sanz Camacho, T. Broux, J. Olchowka, C. Masquelier, L. Croguennec, D. Carlier, *Chem. Mater*. **2019**, *31(23)*, 9759-9768.

[13] J. Serrano-Sevillano, D. Carlier, A. Saracibar, J-M. Lopez del Amo, M. Casas-Cabanas, *Inorg. Chem.* **2019**, *58*, 138347-8356.

[14] K. Momma, F. Izumi, *Journal of Applied Crystallography* **2008**, *41*, 653–658.

[15] B-L. Ellis, T-N. Ramesh, L. Davis, G. Goward, L. Nazar, *Chem. Mater.* **2011**, *23*, 5138–5148

[16] E. Avvakumov, M. Senna, N. Kosova, *Journal of Solid State Electrochemistry* **2014**, *18*, 1389–1399.

[17] M. Bianchini, J-M. Ateba-Mba, P. Dagault, E. Bogdan, D. Carlier, E. Suard, C. Masquelier, L. Croguennec, *J. Mater. Chem. A* **2014**, *2* (26), 10182–10192.

[18] S-S. Parapari, J-M. Ateba Mba, E. Tchernychova, G. Mali, I. Arcon, G. Kapun, M-A. Gülgün, R. Dominko, *Chem. Mater.* **2020**, 32, 262-272.

[19] A. E. Bennett, C. M. Rienstra, J. M. Griffiths, W. Zhen, P. T. Lansbury, R. G. Griffin, *J. Chem. Phys.* **1998**, *108*, 9463–9479.

[20] Y. Ishii, *J. Chem. Phys.* **2001**, *114*, 8473–8483.

[21] A. Castets, D. Carlier, Y. Zhang, F. Boucher, M. Ménétrier, *J. Phys. Chem. C* **2012**, *116*, 18002–18014.